– Supporting Information –

Enhanced Photoelectrochemical Performance of Cuprous Oxide/Graphene Nanohybrids

Egon Kecsenovity[a,b], Balázs Endrődi[a,b], Péter S. Tóth[c], Yuqin Zou[c], Robert A. W. Dryfe[c], Krishnan Rajeshwar[d], Csaba Janáky[a,b,*]

[a] MTA-SZTE „Lendület" Photoelectrochemistry Research Group, Rerrich Square 1, Szeged, H-6720, Hungary

[b] Department of Physical Chemistry and Materials Science, University of Szeged, Rerrich Square 1, Szeged, H-6720, Hungary

[c] School of Chemistry, University of Manchester, Manchester M13 9PL, United Kingdom

[d] Department of Chemistry and Biochemistry, The University of Texas at Arlington, Arlington, Texas 76019, USA

*E-mail: janaky@chem.u-szeged.hu

1. Determination of the electrochemically active surface area of the graphene substrates

Before electrochemical synthesis of the Cu_2O/graphene composites, consecutive potentiodynamic cycling was performed until stable capacitive electrochemical behavior was reached; this ensured proper wetting of the porous graphene structure. The potential window for this pre-conditioning step was chosen so that no Faraday process occurred in this regime (neither with the electrolyte, nor with the electrode itself, see Figure S1).

Similar measurements were performed on a carefully polished, flat glassy carbon electrode, which had the same electroactive and geometrical surface area (i.e., its surface roughness is 1), and thus served as the basis of normalization. The ratio of the charge capacitance (or the charging currents, recorded at a carefully chosen potential, at E = 0.2 V in our case) values directly yielded the ratio of the electroactive surface areas. The used graphene platelets had about six-times higher *specific* surface area than the CNT films (in line with typical surface area data for such materials); therefore smaller loadings were enough to have the same actual electrode surface area. Interestingly, the electroactive surface area of the 3D graphene electrode was considerably smaller than that of the spray coated samples, which will be taken into account in what follows. These measurements were performed for each graphene substrate individually and the measured current values were normalized with respect to the derived surface area when normalized data are presented.

The automated spray-coating resulted in scalable immobilization of the graphene flakes on the ITO surface (Figure S1b). Both the mass and the charge capacitance scaled linearly with the number of spray-coating cycles.

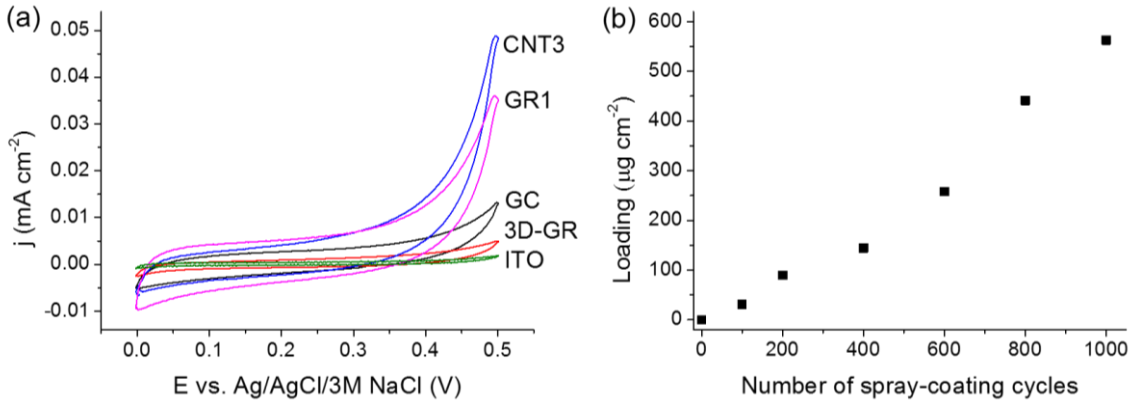

Figure S1. (a) Cyclic voltammograms of the nanocarbon electrodes in 0.1 mol dm^{-3} Na_2SO_4 solution (scan rate: 50 mV s^{-1}). (b) Surface coverage of the graphene-coated electrodes as a function of the spray-coat cycles.

Table S1. Annotation and properties of the studied nanocarbon substrates.

Designation	Spray-coat cycles	Mass (µg cm^{-2})	Surface capacitance (mC cm^{-2})
GR1	100	30	0.078
GR2	200	90	0.238
GR4	600	250	0.661
GR6	1000	560	1.44
CNT3	200	170	0.063
CNT5	800	690	0.257
3D-GR	-	-	0.014

2. Electrodeposition of nanocrystalline Cu_2O on the graphene substrates

As the first step of Cu_2O electrodeposition, linear sweep voltammetry curves were recorded on the various substrates in the electrodeposition solution. As seen in Figure S2, the onset potential of the deposition process was around E = (–0.15) – (–0.20) V for all nanocarbon samples. Based on these results E = –0.25 V was applied for the synthesis of Cu_2O/graphene composites. To ensure complete coverage of the substrate, nuclei formation was initialized by introducing a seed nucleation step at more negative potential (E = –0.35 V) until Q = 100 mC cm^{-2} charge was passed. The vertical dashed lines (Figure S2) indicate the deposition potentials.

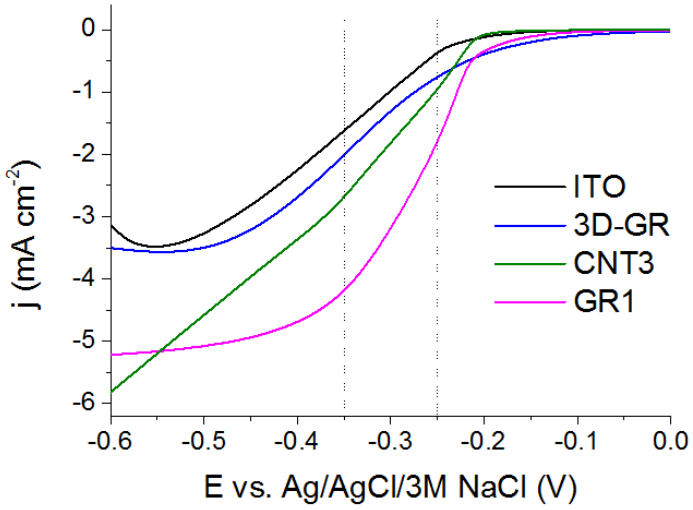

Figure S2. Linear sweep voltammograms, recorded in a basic solution of lactate-stabilized copper sulfate, containing 0.4 mol dm^{-3} cupric sulfate and 3 mol dm^{-3} lactic acid in deionized water at pH = 9. The temperature was kept at T = 60°C, and the solution was vigorously stirred during the synthesis. The sweep rate was 25 mV s^{-1}.

3. Morphological studies of Cu_2O / graphene samples

Additional TEM and SEM images are shown in Figure S3 to further illustrate the homogeneous distribution of the Cu_2O nanocrystallites on the graphene substrates. Images taken at higher magnifications also demonstrated the octahedral shape of the Cu_2O nanoparticles.

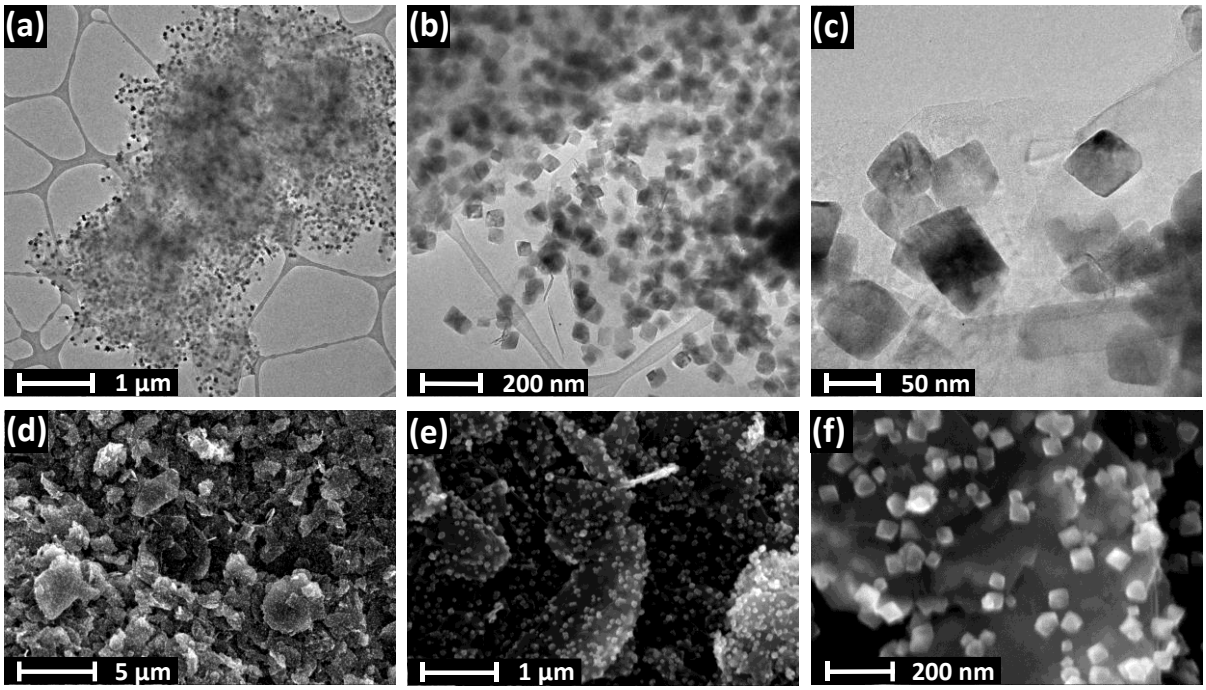

Figure S3. TEM (a-c) and SEM (d-f) images of a Cu_2O/GR hybrid (200 mC cm^{-2}, GR4) captured at various magnifications.

4. Morphology of the bare Cu_2O electrodes

SEM images were taken for the bare Cu_2O film on an ITO electrode. The most important observation is that the crystallite sizes are much larger in this case, due to the smaller electrode surface area (note that the amount of the deposited Cu_2O was identical).

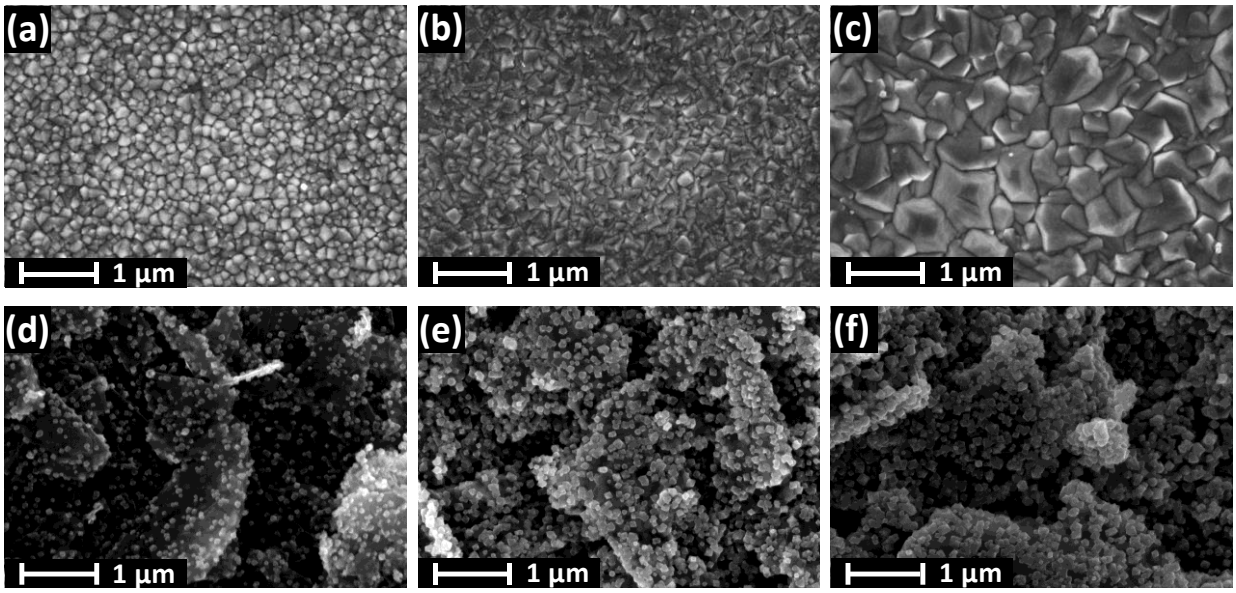

Figure S4. SEM images of Cu_2O (a-c) and Cu_2O/GR4 (d-f) films, deposited with 200 mC cm^{-2} (a, d), 600 mC cm^{-2} (b, e), and 1000 mC cm^{-2} (c, f).

5. Elemental mapping of Cu_2O / 3D graphene substrates

The homogeneity of the Cu_2O coverage on 3D-GR substrate was probed by energy dispersive X-ray microanalysis (EDX). As seen in Figure S5, the graphene plates were homogeneously coated with Cu_2O, when the formerly described two-step electrodeposition protocol was employed.

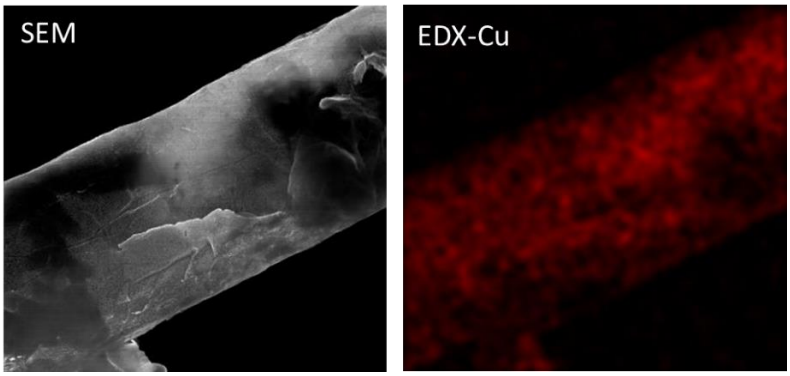

Figure S5. SEM and EDX images of a Cu_2O / 3D-GR graphene composite deposited with 1 C cm^{-2} charge density.

6. XPS analysis of a Cu_2O/GR sample

XPS data confirmed that no Cu was formed during electrodeposition of Cu_2O (see the lack of Cu (0) peak around 918.6 eV in the Auger spectrum, Figure S6B), and interestingly indicated the presence of some CuO (~20%), which might be the result of incipient oxidation of the sample in contact with air after synthesis.

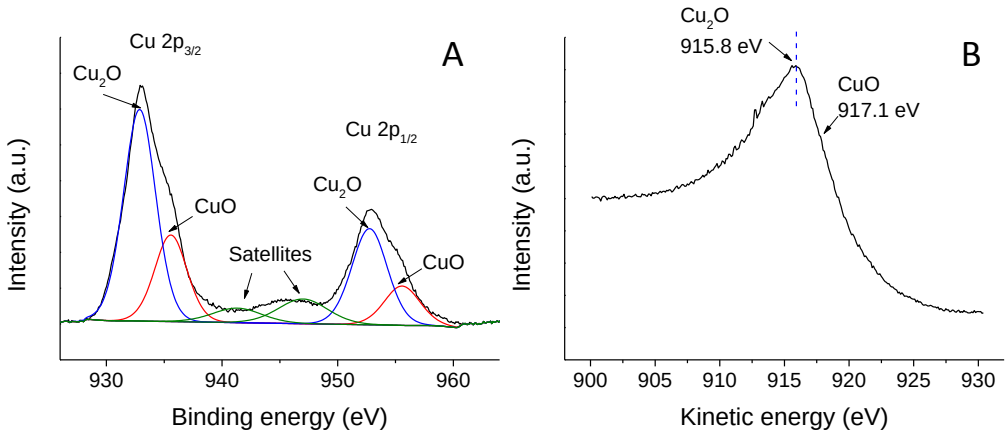

Figure S6. Cu XPS (A) and LMM Auger (B) spectra, recorded for a Cu_2O/GR2 sample.

7. Long-term photoelectrolysis on a bare Cu_2O electrode

Long-term photoelectrolysis was performed using a bare Cu_2O electrode, and the main products were found to be ethanol and methanol, although at a different ratio compared to what was observed for the composite samples. The relative amount of ethanol (vs. methanol)

was smaller in the case of the bare oxide (Figure S7), most likely because of the shorter residence time of the intermediate reduction products (vs. the case of the nanohybrid electrode). This process, however is complex and several other factors (most importantly local potentials) may affect the product distribution, and this question will be further studied in the future.

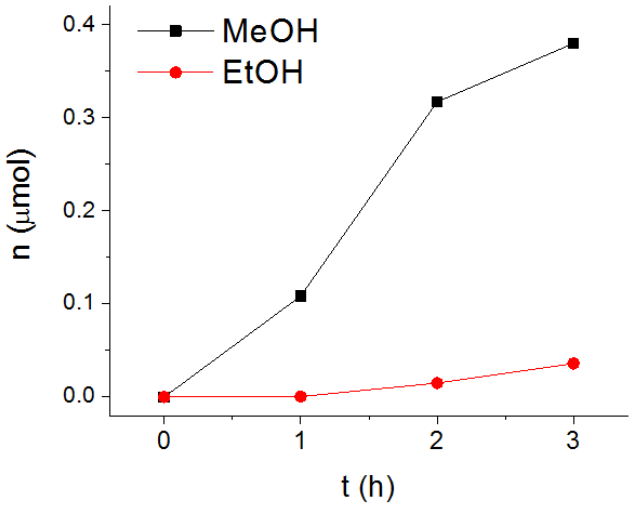

Figure S7. Formation of alcohols during the long-term photoelectrolysis performed on a Cu_2O electrode (1 C cm^{-2}), registered at E= +0.05 V potential (vs. Ag/AgCl/3 M NaCl), in CO_2 saturated 0.1 M Na_2SO_4 solution. A solar simulator was used employing a UV cut-off filter (<400 nm).

8. Photoelectrochemical behavior of Cu_2O/3D-GR composites at different Cu_2O loadings

To demonstrate the decisive effect of the loading on the PEC properties in the case of 3D-GR samples, a set of hybrids was obtained with different composition (0.5 C, 1C, and 2C cm^{-2} deposition charge). These measurements revealed that after reaching a certain oxide thickness, the PEC properties could not be further improved, because the bulk-like behavior of the Cu_2O became dominant. With the notion that the Cu_2O amount in the composite has a decisive effect on the PEC properties, a set of hybrid samples was obtained with different composition (0.5 C cm^{-2}, 1 C cm^{-2}, and 2 C cm^{-2} deposition charge). As seen in Figure S8, after a rapid increase in the photocurrents with the loading, a maximum was reached at 1C cm^{-2} deposition charge. This trend can be explained by complete coverage of the carbon support (also supported by SEM images not shown here); thus further growth of cuprous oxide will result in bulk-like behavior (thus hindering the beneficial effect of the graphene template).

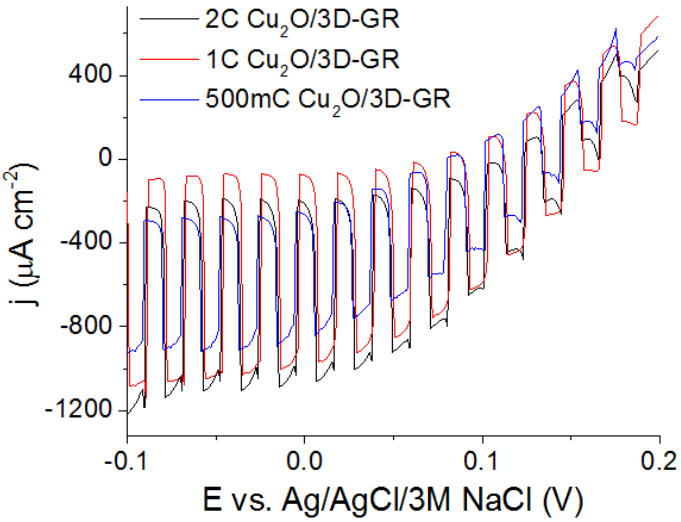

Figure S8. Linear sweep photovoltammograms of Cu_2O/3D-GR composites with varying Cu_2O content, in CO_2 saturated 0.1 mol dm^{-3} Na_2SO_4 solution. The sweep rate was kept at 2 mV s^{-1}, while the light-chopping frequency was 0.2 Hz.

9. Stability of the 3D-GR architecture

Degradation of the Cu_2O/3D-GR electrode structure is a relevant concern. We found that major degradation of the 3D structure only occurred when the photoelectrolysis was performed at more negative potentials, where water splitting (and thus H_2 bubble formation) also occurred. SEM images were taken for samples after photoelectrolysis, and are presented in Figure S9.

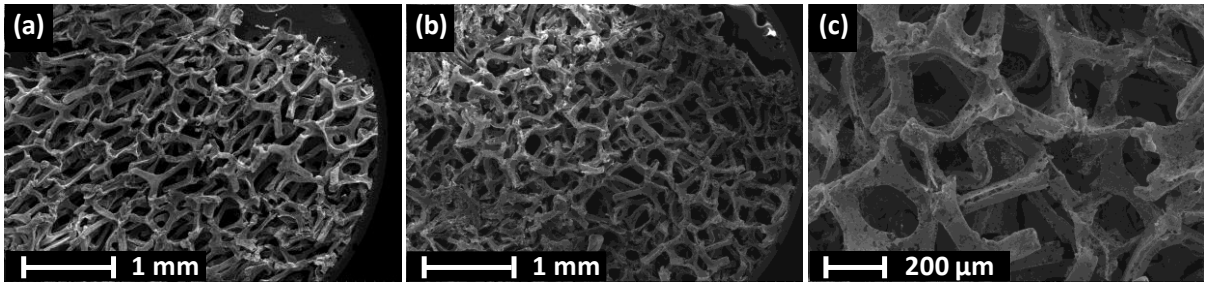

Figure S9. SEM images of a Cu_2O/3D-GR photoelectrode before (a) and after (b, c) long-term photoelectrolysis.

10. Electrochemical Impedance Spectroscopy of Cu_2O/graphene samples

The recorded EIS data were fitted and analyzed using the equivalent circuit shown in Figure S6. The elements of the circuit are the following: series resistance (R_s), charge transfer resistance (R_{ct}), double layer capacitance related to the high surface area of the porous electrode (C_1), a diffusion related Warburg element (W) and another capacitance (C_2) completed the modified RRC-circle.

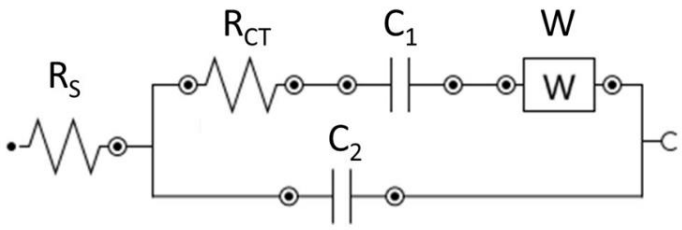

Figure S10. The employed equivalent circuit to fit the EIS data.

11. Analysis of the flatband potential of the electrodes

To compare the flatband potential (and thus the apparent Fermi level) of the photoelectrodes, Table S2 summarizes the onset potential of the photovoltammetry profiles, the open circuit potentials (OCPs) with and without illumination, and the flatband potential obtained from the Mott-Schottky plots. The most important trend observed in these comparisons was the slight positive shift in the flatband potential (apparent Fermi level) in the case of the composite samples (compared to the bare Cu_2O). The magnitude of this shift increased with increasing nanocarbon loading, and had a maximum of 100 mV for the spray-coated carbons and 200 mV for the 3D-GR sample. These shifts indicate the intimate contact between the constituents, similar to trends in other studies in the literature on different semiconductor/nanocarbon assemblies (see refs. #30,31,33, and 64 in the main text).

For easier comparison, the potentials are compared at the RHE scale. Data were obtained using the following equation: $E_{RHE} = E_{Ag/AgCl} + 0.059\ pH + E^{o}_{Ag/AgCl}$

Table S2. Comparison of the flatband potential obtained via different methods

Support	**OCP (dark) E vs. RHE (mV)**	**OCP (light) E vs. RHE (mV)**	**Photovoltammetry onset E vs. RHE (mV)**	**FB from Mott-Schottky E vs. RHE (mV)**
ITO	447	622	747	1015
GR2	445	623	703	1016
GR4	436	618	717	1020
GR6	465	605	728	1104
CNT	415	620	696	1084
3D-GR			755	1230

12. Photocurrent Transient Analysis

Before analyzing the composite samples, the photocurrent transients of bare Cu_2O films were studied. As seen in Figure S11, gradually larger τ_1 values were obtained with higher oxide thicknesses. The effect of CO_2 was also demonstrated, when higher steady-state photocurrents and τ_1 values were detected in the presence of CO_2 (compared to measurements in N_2 saturated solutions, Figure S11b).

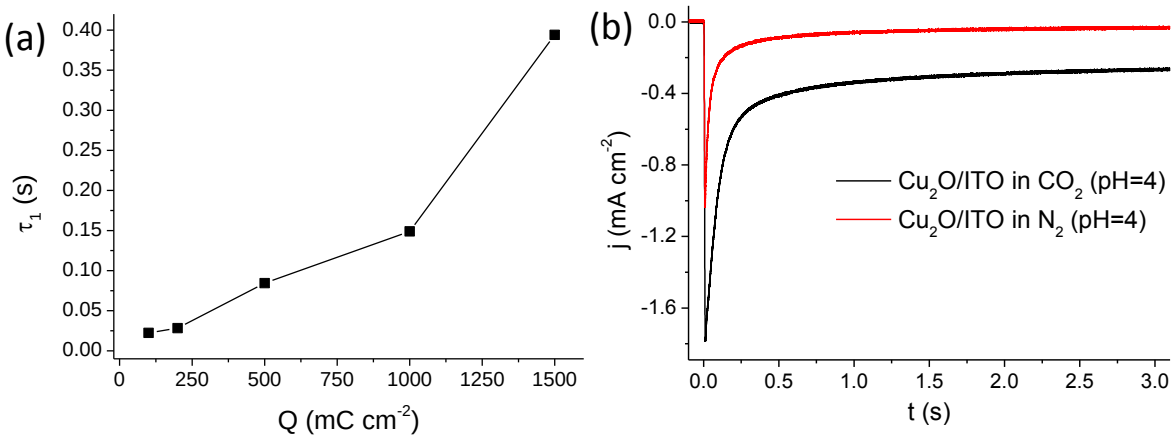

Figure S11. (a) τ_1 values determined for Cu_2O/ITO films with different oxide thickness. (b) transient photocurrent measurements for a Cu_2O/ITO film (0.5 C cm^{-2}) in CO_2 or N_2 saturated 0.1 mol dm^{-3} Na_2SO_4, and N_2 saturated buffer solution, having the same pH as CO_2 saturated aqueous solutions (pH = 4.0).

13. Comparison of the PEC behavior of photoelectrodes with different nanocarbons

In addition to the transient photocurrent measurement shown in Figure 11, photocurrent transients are also shown for two pairs of photoelectrodes with very similar surface area (see Table S1), but different nanocarbons (graphene and CNT). As seen in Figure S12, graphene seems to provide better charge separation (i.e., longer recombination times) compared to CNT. At higher loadings, this also results in notably higher stationary currents, most likely because of the smaller number of carbon/carbon interfaces (note the different morphological attributes of CNT and graphene).

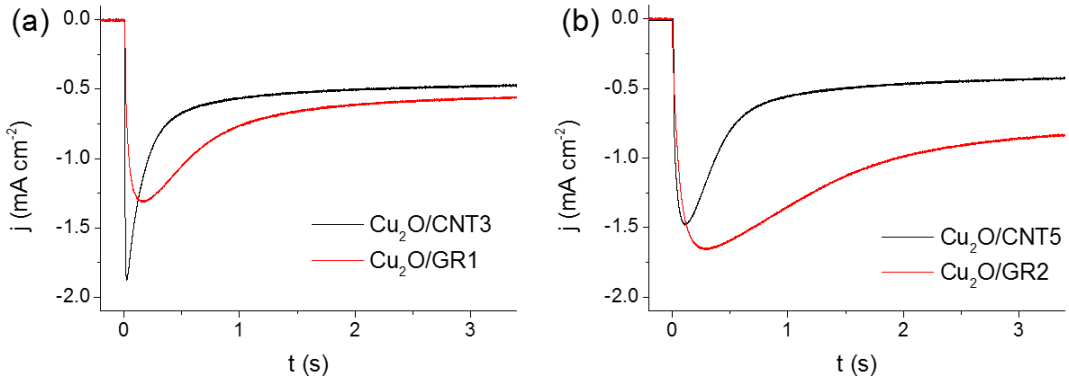

Figure S12. Photocurrent transient analysis of different Cu_2O/nanocarbon composites deposited with 0.5 C cm^{-2} charge density. The measurements were performed in CO_2 saturated 0.1 M Na_2SO_4 solution at E = 0.05 V potential. A solar simulator with a UV cut-off filter (<400 nm) was used.